Photonic band structure of bcc colloidal crystals

Ranjit D. Pradhan, John A. Bloodgood, and George H. Watson
Department of Physics and Astronomy, University of Delaware, Newark, Delaware 19716
(Received 10 October 1996)

Self-ordering colloidal systems are being recognized as possible candidates for optical photonic crystals. Such structures exhibit three-dimensional periodicity in refractive index, and possess lattice dimensions comparable to optical wavelengths. Recently, fcc colloidal crystals of water-suspended polystyrene microspheres were investigated in the context of photonic band structure. At lower polystyrene volume fractions, these colloidal suspensions crystallize in the bcc crystal lattice. This work extends our investigation of this system to cover the bcc phase and reiterates the use of Kossel lines in mapping the underlying photonic band structure. Along certain crystal directions, numerous Kossel lines intersect, giving rise to unusually large optical stop bands. [S0163-1829(97)00216-6]

Periodicity of a dielectric medium can have a profound effect on the electromagnetic waves which propagate through it. Such a medium, the so-called photonic crystal, can forbid photon transport for a certain band of frequencies irrespective of polarization or propagation direction, leading to a complete photonic band gap (PBG).[1,2] In the optical regime such a structure is projected to have a deep impact on a wide range of photonic applications, many relying on the suppression of spontaneous emission in a PBG material.[3]

In principle, one can produce a structure with a complete PBG in the optical regime by scaling lattice parameters of known PBG structures to optical wavelengths. However, technological constraints have impeded the realization of this goal. To our knowledge, the smallest wavelength at which a complete three-dimensional PBG has been demonstrated to date is roughly 500 μm.[4]

Self-organizing colloidal crystal systems provide a means of generating periodic dielectric structures with feature sizes comparable to optical wavelengths. Full three-dimensional PBG's have not yet been demonstrated in these systems because of the high contrast demanded in the index of refraction. Nevertheless, they serve as a suitable platform for the study of photonic band-structure effects from the infrared to the visible regime.[5–10] The photonic band structure of fcc polystyrene colloidal crystals has been studied extensively along a number of symmetry directions.[8,9] At lower polystyrene volume fractions, the colloidal suspension crystallizes in the bcc phase, which is the subject of this paper.

Kossel line patterns can reveal the underlying photonic band structure of colloidal crystals.[9] These patterns can be generated by passing a monochromatic laser beam through a single colloidal crystal. Disorder, which is present in colloidal crystals in the form of dispersion in polystyrene microsphere diameter, vacancies, and other lattice imperfections, helps generate diffuse light which Bragg diffracts from the crystal planes. This diffraction leads to the formation of Kossel line patterns, both in transmission and reflection. These patterns aid in locating and identifying the symmetry directions of the crystal. In this work, we reinforce the close connection between the optical stop bands in colloidal crystals and their associated Kossel lines.

The colloidal crystals for this study were prepared by diluting suspensions of charged polystyrene microspheres with a diameter of 0.110 nm to obtain a volume fraction of 1.0–1.2 %. The phase diagram for this system[11] suggests that for 0.110-nm microspheres one expects crystallization in the bcc phase for volume fractions below 3%. However, for samples with volume fractions just under 3%, Kossel lines indicate significant patches of fcc crystallites in a bcc background. Also, while samples with volume fractions under 1% are purely bcc, the optical stop bands of these samples are somewhat shallow. The best compromise between obtaining adequate stop bands and avoiding fcc crystallites occurs at volume fractions near those chosen for this study. The crystals were prepared in specially fabricated cells using a procedure described elsewhere.[10] Shear annealing[12,13] facilitates the formation of mm-sized single crystals which preferentially orient with their bcc (110) planes parallel to the glass windows of the crystal cell. Kossel lines were observed for wavelengths between 465 and 615 nm using a R6G-based dye laser. The Kossel lines shown in this paper were simulated using a program obtained from Weber, Schetelich, and Greist.[14] The transmission spectra through these crystals were obtained along a number of symmetry directions using a modified UV/visible/near-IR spectrophotometer. We estimate the wavelength uncertainty in our spectrophotometer transmission measurements to be within ± 0.5 nm.

In this work we map the photonic band structure of bcc colloidal crystals from the N point to the P point. These symmetry points are shown in Fig. 1(a), which shows the first Brillouin zone (FBZ) of the bcc lattice. The N point corresponds to the [110] direction, while the Γ point is at the center of the FBZ. For a bcc crystal the 12 faces of the FBZ correspond to the 12 planes of the {110} family. The P point is located at the intersection of three faces of the FBZ, corresponding to three of the {110} planes. Similarly, the H point is located at the intersection of four faces of the FBZ, corresponding to four of the {110} planes. The incident beam must pass at an angle of 35° in the crystal (50° in air) relative to the [110] direction to access the P point and at an angle of 45° in the crystal (78° in air) to access the H point. The large incidence angle of 78° in air presents experimental difficulties in accessing the H point; however, the P point is readily accessible.

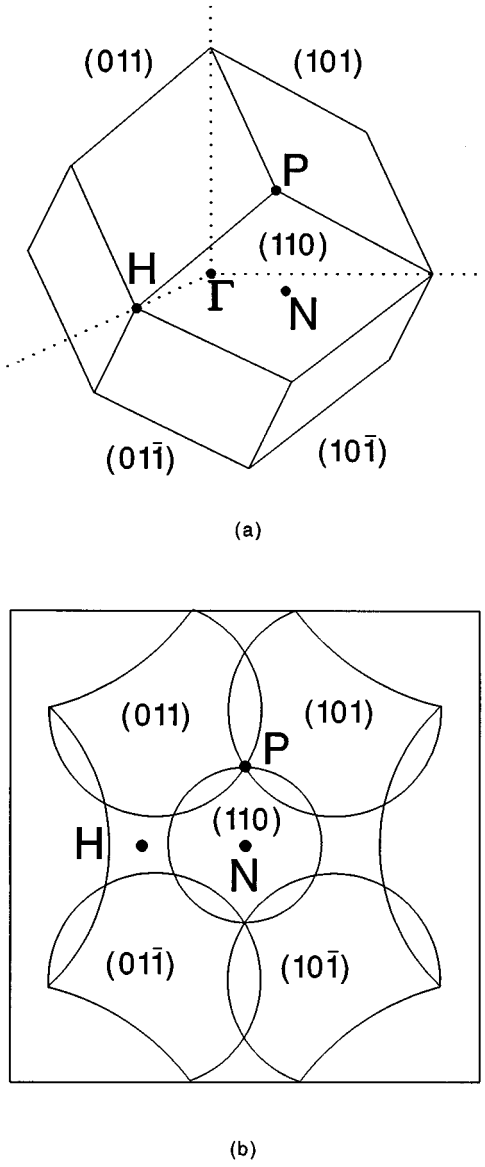

FIG. 1. The bcc first Brillouin zone (FBZ): The bcc FBZ (a) is shown along with a Kossel line simulation at 555 nm in the crystal (b). The pattern shown is a 180° stereographic projection of the hemispherical Kossel line image. The Kossel lines shown are for a bcc crystal with a lattice parameter of 480 nm. The symmetry of the FBZ is reflected in the Kossel line projection.

Figure 1(b) shows the Kossel line simulation for a bcc crystal along the [110] direction at a crystal wavelength of 555 nm (741 nm in air). The lattice parameter was chosen to be 480 nm. An incident beam along the [110] direction would pass through the center (*N* point) of the Kossel line simulation. The rings shown in the Kossel line simulation shrink in diameter with increasing wavelength. When a Kossel line is located at the center of the pattern, the incident beam Bragg diffracts, forming an optical stop band in the transmission spectrum. The 741-nm wavelength being out of the range of our dye laser, this pattern was not observed directly. However, at shorter wavelengths the rhombus-shaped symmetry of the (110) face of the FBZ can be seen in the Kossel line pattern. This symmetry was used to identify the orientation of the Γ-*N*-*P* plane. The *P* point can then be

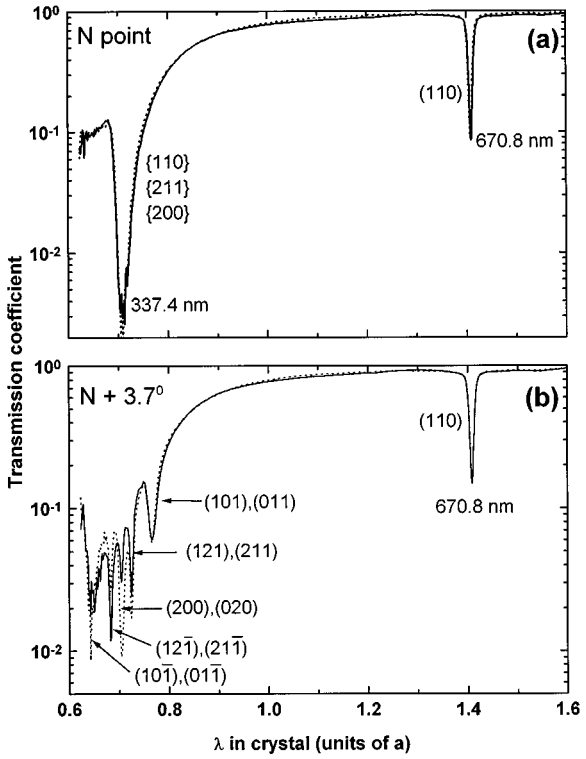

FIG. 2. Transmission spectra near the [110] direction (*N* point). The first spectrum (a) shows the [110] transmission through a crystal with a lattice parameter of 476.4 nm. Notice the significantly wider and deeper optical stop band at 337.4 nm. The second spectrum (b) is taken at an incidence direction of 3.7° relative to the [110] direction. The 337.4-nm stop band separates into its constituent stop bands with the slightest departure from the [110] direction. The solid lines correspond to the case of vertical polarization (polarization perpendicular to the *N*-*P* direction), while the dotted lines correspond to the case of horizontal polarization.

accessed by rotating the crystal 50° in air from the *N* point.

Figure 2(a) shows the experimental transmission spectrum along the [110] direction of a crystal with a lattice parameter of 476.4 nm. The wavelength in the crystal is expressed in units of the lattice parameter a. Unavoidably, the lattice parameter of each crystal varied from sample to sample. Our crystals possessed lattice parameters between 476.4 and 484.8 nm. To reduce the effect of this variation on our results, the lattice parameter was extracted from the wavelength of the first-order stop band along the [110] direction, as described in Ref. 10. The wavelength was then normalized with the extracted lattice parameter. The scale invariance of Maxwell's equations allows for such a normalization, which is convenient for comparing crystals of slightly different lattice parameter. However, this does not remove the effect of variation in the volume fraction, which is expected to result in a small variation in the widths of optical stop bands.

In Fig. 2(a) the optical stop band at 670.8 nm ($\sim$893 nm in air) is due to first-order Bragg diffraction of the incident beam from the (110) planes. This stop band can be interpreted in terms of the Kossel line pattern shown in Fig. 1(b). The central (110) ring reduces in diameter with increasing wavelength, and finally collapses onto the incident beam at the (110) stop-band wavelength (670.8 nm in the crystal). Second-order Bragg diffraction, expected at about half the

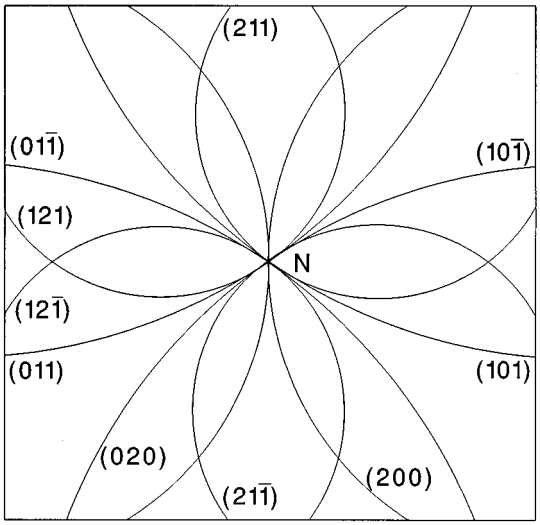

FIG. 3. Multiple Kossel lines intersecting to produce the unusually large optical stop band seen in Fig. 2(a). The Kossel line simulation shown here is a 90° stereographic projection for a crystal with a lattice parameter of 480 nm at a wavelength of 339 nm in the crystal. The Kossel rings intersecting at the center of the frame are due to the following planes: (01$\bar{1}$), (101), (10$\bar{1}$), (011), (211), (12$\bar{1}$), (121), (21$\bar{1}$), (200), and (020). This results in the unusually deep and wide optical stop band seen along the [110] direction (N point) at 337.4 nm [Fig. 2(a)].

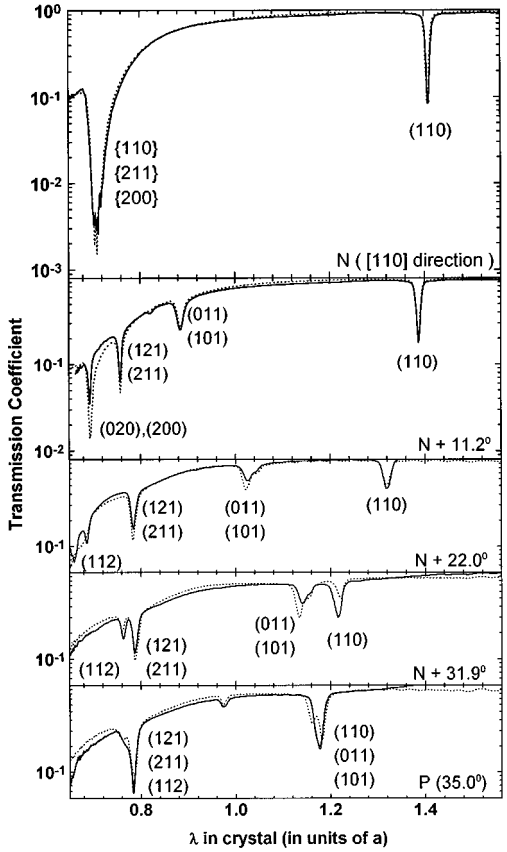

FIG. 4. Transmission scans from the N point to the P point. Going from the N point to the P point involves rotating the incident wave vector $\vec{k}$ inside the crystal through an angle of 35.0°. This necessitates rotating the crystal by an angle of 50° in air relative to the [110] direction. The transmission curves are shown for the 0.0° (N point), 11.2°, 22.0°, 31.9° and 35.0° (P point) incidence angles in the crystal. These correspond to incidence angles of 0.0°, 15.0°, 30.0°, 45.0° and 50.0° in air (0° corresponds to the [110] direction). The solid lines are the transmission scans for the case of vertical polarization (polarization perpendicular to the N-P direction), while the dotted lines represent the case of horizontal polarization.

wavelength of the first-order diffraction, is usually weaker. Therefore, at first glance, it is surprising that the stop band seen at 337.4 nm (~453 nm in air) is considerably deeper and wider than the first-order stop band. However, an examination of the expected Kossel lines at this wavelength (Fig. 3) reveals that this stop band owes its depth to Bragg diffraction from several sets of crystal planes. In addition to the second-order diffraction from the (110) planes, a multitude of other planes contribute to the diffraction of the incident beam at this wavelength. These include four sets of planes from the {110} family, four sets from the {211} family and two sets from the {200} family. This demonstrates that even in low dielectric contrast crystals, significant reduction in the transmission coefficient can result from the intersection of multiple Kossel lines at the incidence axis. By rotating the crystal away from the [110] direction by a small angle, the individual contributions to the 337.4-nm stop band may be resolved. Figure 2(b) shows the transmission spectrum when the beam is incident at an angle of 3.7° in the crystal (5.0° in air). The 337.4-nm stop band has separated into multiple stop bands. As shown in Fig. 3, many Kossel lines intersect the incident beam at 337.4 nm along the [110] direction. Along any other direction, the symmetry of the [110] direction is broken, regardless of wavelength. That is, as the Kossel rings shrink in diameter with increasing wavelength, they separately cross any point slightly displaced from the N point. Therefore it is possible to resolve the individual contributions by taking transmission scans along an off-[110] direction, as shown in Fig. 2(b).

Figure 4 shows transmission spectra along several directions between the N and P points. Each of the stop bands corresponds to the intersection of a Kossel line and the incident beam, as shown in Fig. 5. The first, second, third, and fourth rows of Fig. 5 correspond to the 11.2°, 22.0°, 31.9°, and 35.0° spectra in Fig. 4, respectively. The arrows in Fig. 5 start from the N point and point in the direction of the P point. The short segment intersecting each arrow indicates the point where the incident beam passes the screen. The intersection of a Kossel line and the incident beam results in the formation of a stop band in the transmission spectrum. The first row of Fig. 5 contains four frames, which correspond to the four stop bands shown in the 11.2° transmission scan of Fig. 4. The last row contains only two frames, which correspond to the two stop bands in the 35.0° scan of Fig. 4. The small feature which appears between the two major stop bands in the 35.0° scan is believed to be an artifact. The feature grows with increasing angle beyond 50.0° in air. We believe that at such large angles the incident beam transgresses into a neighboring crystallite which has a different orientation from the one being investigated. In the rightmost column of Fig. 5, the wavelength inside the crystal successively increases from 555 (lowermost frame) to 665 nm (up-

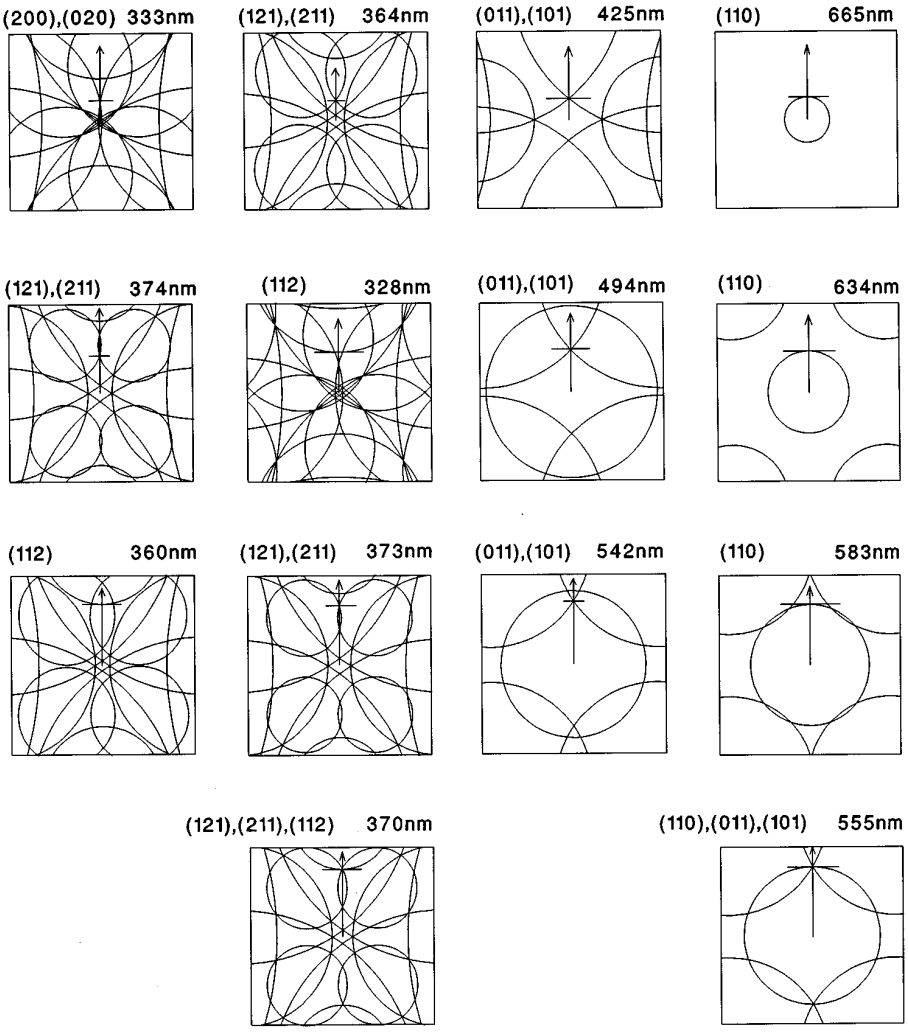

FIG. 5. 90° stereographic projections of the Kossel line patterns at wavelengths ranging from 328 to 665 nm. The four rows of frames correspond to the four lowermost transmission spectra of Fig. 4. The wavelength in the crystal for each pattern is indicated above the corresponding frame. The arrow in each frame originates at the *N* point and indicates the direction from the *N* point to the *P* point. The intersection of the short segment and the *N*-*P* line (cross-hair) indicates the direction of the probe beam used to obtain the transmission spectra in Fig. 4. The crossing of a Kossel line over the direction of incidence generates a stop band in the corresponding transmission spectrum. The plane(s) indicated above each frame are those which correspond to the Kossel lines intersecting at the cross-hairs.

permost frame). The [110] circle can be seen to shrink in diameter with increasing wavelength and is expected to reduce to a point which intersects the incident beam at 679 nm in the [110] direction. In the first and second columns, the Kossel lines are considerably dense owing to the presence of second Brillouin-zone Kossel lines in addition to those from the FBZ. The FBZ of the bcc lattice, shown in Fig. 1(a), is less spherical than the FBZ of the fcc lattice. Consequently, many regions of the second Brillouin zone are likely to be located within the shell in *k* space corresponding to the wavelength range of interest. This results in a narrowing of the separations between the stop bands of the first and second Brillouin zones, producing intricate Kossel line patterns.

Figure 6 shows a mapping of the photonic band structure for bcc polystyrene colloidal crystals from the *N* point to the *P* point. Merging of the (110), (011), and (101) stop bands occurs at the *P* point. In addition, the (121), (211), and (112) stop bands merge at this propagation direction, but at a shorter wavelength. The dotted curves indicate the photonic band structure obtained from the Kossel line simulations, which represents a band-structure mapping based purely on the Bragg law. The hollow and filled symbols show our results for vertically and horizontally polarized spectrophotometer beams. The horizontally polarized beam is polarized paralled to the *N*-*P* direction. In the case of photonic crystals, the Bragg law is only an approximation.[15] However signifi-

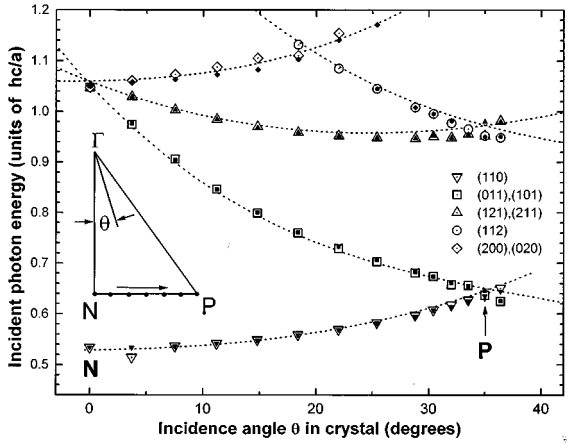

FIG. 6. Photonic band structure of bcc colloidal crystals obtained from the transmission measurements shown in Fig. 4. The incident photon energy is expressed in units of hc/a. This is compared with the photon energy calculated (dotted lines) from the Kossel line simulations, which are based purely on the Bragg law. The hollow symbols correspond to the planes indicated in the figure for the case of vertical polarization, and the corresponding solid symbols refer to the case of horizontal polarization. The inset shows the cross section of the bcc FBZ, indicating the angle of incidence θ in the crystal.

cant departures from the Bragg law are not expected in a crystal with such a low contrast in the index of refraction. As seen in Fig. 6, the experimental data closely follows the curves predicted by the Bragg law. The two bands of lowest energy correspond to diffraction from families of planes of the FBZ. The bands corresponding to diffraction from the {121} and {200} families of planes are not sufficiently separated in energy from the FBZ bands, leading to a crowding of Kossel lines not normally seen in the fcc structure.

In conclusion, we have presented a mapping of the photonic band structure of bcc colloidal crystals from the *N* point to the *P* point, highlighting the role of Kossel lines in revealing the photonic band structure. In particular, we demonstrated the role of multiple-intersecting Kossel lines in producing unusually large optical stop bands in a system with a relatively low contrast in refractive index. Since the bcc FBZ is highly nonspherical, Kossel lines arising from the second Brillouin zone appear in the same wavelength range as the FBZ Kossel lines along certain directions. This increases the probability for the multiple intersection of Kossel lines, which can produce large optical stop bands.

We acknowledge helpful discussions with Dr. İ. İnanç Tarhan. J.A.B. would like to acknowledge summer support from the Laser Science Topical Group of the American Physical Society under the program of Undergraduate Research Support in Laser Science. This work was supported by the National Science Foundation under Grant No. DMR-9510460.

[1] Special review issues: C. M. Bowden, J. P. Dowling, and H. O. Everitt, J. Opt. Soc. Am. B **10**, 279 (1993); G. Kurizki and J. W. Haus, J. Mod. Opt. **41** (1994).

[2] For a recent review, see *Photonic Band Gap Materials*, edited by C. M. Soukoulis (Kluwer, Dordrecht, 1996).

[3] E. Yablonovitch, J. Mod. Opt. **41**, 173 (1994).

[4] E. Özbay, E. Michel, G. Tuttle, R. Biswas, K. M. Ho, J. Bostak, and D. M. Bloom, Opt. Lett. **19**, 1155 (1994).

[5] J. Martorell and N. M. Lawandy, Phys. Rev. Lett. **66**, 887 (1991).

[6] C. J. Herbert and M. S. Malcuit, Opt. Lett. **18**, 1783 (1992).

[7] V. N. Bogomolov, D. A. Kurdyukov, A. V. Prokof'ev, and S. M. Samolĭlovich, Pis'ma Zh. Eksp. Teor. Fiz. **63**, 496 (1996) [JETP Lett. **63**, 520 (1996)].

[8] İ. İ. Tarhan, M. P. Zinkin, and G. H. Watson, Opt. Lett. **20**, 1571 (1995).

[9] İ. İ. Tarhan and G. H. Watson, Phys. Rev. Lett. **76**, 315 (1996).

[10] R. D. Pradhan, İ. İ. Tarhan, and G. H. Watson, Phys. Rev. B **54**, 13 721 (1996).

[11] P. A. Rundquist, P. Photinos, S. Jagannathan, and S. A. Asher, J. Chem. Phys. **91**, 4932 (1989).

[12] N. A. Clark, A. J. Hurd, and B. J. Ackerson, Nature (London) **281**, 57 (1979).

[13] P. Pieranski, Contemp. Phys. **24**, 25 (1983).

[14] S. Weber, Ch. Schetelich, and V. Greist, Cryst. Res. Technol. **29**, 727 (1994).

[15] W. L. Vos, R. Sprik, A. van Blaaderen, A. Imhof, A. Lagendijk, and G. H. Wegdam, Phys. Rev. B **53**, 16 231 (1996).